Mode couplings and resonance instabilities in finite dust chains

Ke Qiao,* Jie Kong, Lorin S. Matthews, and Truell W. Hyde†
Center for Astrophysics, Space Physics and Engineering Research, Baylor University, Waco, Texas 76798-7310, USA
(Received 19 February 2015; revised manuscript received 24 April 2015; published 8 May 2015)

Employing a numerical simulation, the normal modes are investigated for finite, one-dimensional horizontal dust chains in complex plasma. Mode couplings induced by the ion flow within the sheath are identified in the mode spectra and the coupling rules are determined. Two types of resonance-induced instabilities are observed, one bidirectional and one unidirectional. Bidirectional instability is found to cause melting of the chain with the melting proceeding via a two-step process which obeys the Lindemann criterion. The relationship between the normal mode spectra observed in finite systems and the wave dispersion relations seen in larger systems was also examined using a dust chain model. For this case, the dispersion relation was obtained through multiplication of the mode spectra matrix by a transition matrix. The resulting dispersion relations exhibit both the general features observed in larger crystals as well as several characteristics unique to finite systems, such as discontinuities and strong energy-density fluctuations.

DOI: 10.1103/PhysRevE.91.053101 PACS number(s): 52.27.Lw, 52.35.Mw, 64.60.an, 36.40.Mr

I. INTRODUCTION

Normal modes are used to describe the basic dynamics of physical systems near equilibrium and the analysis of these modes is a fundamental tool employed across various fields of research including molecular chemical physics [1,2], fiber optic physics [3], geophysics [4], and plasma physics [5]. In an ideal linear conservative system, the normal modes are independent of one another. However, real systems are nonlinear and dissipative in nature; thus the normal modes are in general coupled to each other, i.e., there are interactions between them. Mode coupling is therefore a fundamental mechanism for many interesting phenomena such as energy transfer in polyatomic molecules [1,2] or the internal resonance in nonlinear dynamical systems [6,7]. The latter of these is the mechanism leading to ergodicity, which is the underlying foundation for statistical mechanics [6,7].

In the area of complex plasmas, mode coupling was predicted for an infinite plasma crystal [8,9] between the in-plane longitudinal [10,11] and out-of-plane transverse dust lattice wave (DLW) [12–14]. The ambient ion flow in the plasma sheath, where dust particles are levitated and the resulting ion wake below the particles [15–17] can dramatically enhance such coupling mechanisms from second (nonlinear) to first (linear) order [18], allowing detection even at low-amplitude particle displacements. Using a point charge model [8,9,19–22] to simulate the ion wake, it has been shown that resonance instability can be triggered when the two coupled wave modes intersect. This phenomenon was recently observed experimentally [18,23–25] in the thermal fluctuation spectrum illustrated by a high-energy-density region at the intersection between the DLWs. This enhanced energy density corresponds to the resonance instability and can result in melting of the plasma crystal at low neutral gas pressures [23–26].

Recently, research on mode couplings has been extended to include two-dimensional (2D) dust clusters both theoretically [20–22,27] and experimentally [28]. Instead of the continuous high-energy-density region observed in the thermal fluctuation spectrum for large crystals, normal mode spectra for dust clusters exhibit a complex coupling pattern between discrete horizontal and vertical modes even when the modes are not in resonance. In this case, such coupling occurs only between modes having specified symmetries and obeying specific mode coupling rules, similar to the mode coupling seen in polyatomic molecules [1,2]. The instabilities created by the resonance between two coupled modes are discrete, reflecting the discreteness of the normal modes [22,28].

Similar to large crystals, if the resonance instabilities are strong enough, they can induce melting of the cluster with the melting obeying the Lindemann criterion [22]. It is worth noting that although melting and/or the solid-liquid transition is a concept originally defined for large physical systems, it has recently become a topic of increasing interest for finite systems [29,30] and has been observed across a wide variety of systems including electrons in quantum dots [31], ions in traps [32], atomic clusters [33,34], and complex plasmas [35–37]. A theoretical generalization redefining melting in terms of the (thermodynamic) phase space for small systems was recently proposed by Proykova and Berry [34] but there are still many open questions.

In this research, mode couplings and the resulting instabilities and melting are investigated for a one-dimensional (1D) horizontal finite chain formed within a complex plasma and consisting of three to 20 dust particles. Unlike the circular dust clusters previously studied, the chains exhibit no degeneracy between modes due to their anisotropic nature, resulting in different characteristics in mode coupling, resonance instabilities, and melting. The resulting normal mode eigenvectors resemble waves with various numbers of wavelengths, allowing such normal modes in finite systems to be compared to the waves observed in larger systems. More importantly, there are a number of other systems exhibiting chainlike structures, such as polyatomic molecules or proteins, in which the dynamics of mode couplings plays a major role. Unfortunately, mode analysis for these systems is difficult due to their time scale (picoseconds) and length scale (nanometers). Thus, a proper study of complex plasma dust chains provides the potential

*ke_qiao@baylor.edu
†truell_hyde@baylor.edu

to model mode coupling as well as other functions in such microscopic complex systems on a macroscopic time and length scale.

II. METHOD

In this work, the ion wake is modeled employing an adaptation of the widely used point charge model [8,9,19–22]. This model assumes the potential around a dust particle levitated in a plasma sheath to be described by a combination of two potentials, one created by the dust particle with charge Q and another by a positive point charge q located a distance l beneath it, representing the ion wake. Both of the potentials assume a screened Coulomb (Debye-Hückel or Yukawa) form [20–22], as given by

$$U(r) = Q\frac{\exp(-|r - r_Q|/\lambda)}{|r - r_Q|} - q\frac{\exp(-|r - r_q|/\lambda)}{|r - r_q|}, \quad (1)$$

where λ is the screening length and r_Q and r_q are the real and virtual particle positions, respectively. This model provides a reasonable analytical approximation while offering the advantage of highlighting qualitative features of the physical process, such as the positive space charge effect beneath the dust particle.

In a typical experiment on earth, dust particles are assumed to be confined in the vertical direction within the potential well formed by the electrostatic field and gravity, and in the horizontal direction by the electric field produced by the experimental setup [38]. In this case, the external forces acting on the particles are

$$\begin{aligned} F_{z,\mathrm{ext}} &= E_z(x,y,z)\,Q - Mg, \\ F_{x(y),\mathrm{ext}} &= E_{x(y)}(x,y,z)Q, \end{aligned} \quad (2)$$

where x, y, and z are representative particle coordinates. The electric field is assumed linear for small oscillations; thus $E_z = E_0 + E_z'z$, $E_x = E_x'x$, and $E_y = E_y'y$, where E_0 is the vertical electric field at the equilibrium position. Since this research is focused on determining the effects created by the ion wake, other mechanisms such as charge variation are ignored. (Such charge variations do not change the results qualitatively but do renormalize the mode couplings [9].) Therefore, the particle charge Q remains constant and the forces in Eq. (2) constitute a parabolic potential well in both the vertical and horizontal directions [38,39].

An N-body code, BOX_TREE [13,14,21,22,27,40,41], was employed to simulate the dynamics of the dust system. Given the small number of particles, the force on each particle due to all other particles may be calculated directly from the potential given in Eq. (1). All simulations assume an initially random distribution of particles within a box of $10 \times 10 \times 10$ mm^3. The center of mass of the particle system is located at the center of the box, which is also defined as the origin of the coordinate system. Simulation parameters are chosen to represent normative experimental values, with a particle diameter $d = 8.89$ μm, a particle density of 1.51 g/cm^3, a particle charge $Q = 3.5 \times 10^{-15}$ C (22 000e), and a screening length $\lambda = 500$ μm. The ion wake is modeled by assuming a point charge q of magnitude $Q/4$ to $Q/8$, located a distance $l = \lambda/2$ below the dust particles. In order to form a horizontal chain, the confinement in the horizontal plane is fixed at $E_x' = 5 \times 10^4$ V/m^{-2} and $E_y' = 3 \times 10^6$ V/m^{-2}, providing horizontal oscillation frequencies of $f_x = 2.9$ Hz and $f_y = 22.3$ Hz. The vertical confinement E_z' is allowed to vary from $\sim 1.5 \times 10^5$ to 3.5×10^6 V/m^{-2} ($f_z \approx 4.9 \sim 24$ Hz).

To establish stability, the particle system is initially cooled through friction as defined by $F_f = -\mu M\,\boldsymbol{v}$, where $\boldsymbol{v}$ is the particle velocity and $\mu = 10$ s^{-1}. A heat bath, created by elastic random collisions between the dust particles and the ambient gas particles [21,22] and representing a temperature of 1 K, allows mutual particle interactions to dominate the inherent thermal motion. Friction is removed after formation of a stable horizontal chain along the x direction, though the system remains in the heat bath.

Particle oscillations were tracked for approximately 16.67 s with each particle's position and velocity saved at intervals of 1/60 s. Mode spectra were obtained employing the technique used in [21,22,28,42], where the time series of the particle velocities is projected onto the direction of the eigenvectors corresponding to each pure mode (i.e., modes calculated while disregarding the ion wake effect). The normal mode spectrum was then obtained through a Fourier transformation over time.

III. RESULTS AND DISCUSSION

A. Mode couplings

Due to the one-dimensional nature of the system, the $3N$ normal modes (with N defined as the particle number) can be equally divided into x, y, and z modes, with their eigenvectors directed along the x, y, and z axes, respectively. Figure 1 shows the x, z, and y mode eigenvectors for a seven-particle chain. As can be seen, the normal modes in this case resemble a series of nonuniform standing waves with differing numbers of unequal wavelengths. Sorting the eigenvectors in ascending order by number of wavelengths provides a natural index for the modes. In our case, the modes in the three directions will be denoted by $x(n)$, $y(n)$, and $z(n)$ referring to the nth x, y, or z mode, respectively. Here the first x, y, or z mode, corresponding to motion of all particles as a whole, is also called a sloshing mode. It can also be seen that eigenvectors for each of these three mode types exhibit the same patterns. In other words, eigenvectors corresponding to the ith x, y, or z mode have the same magnitude (if normalized) at each particle position, no matter whether their direction is along the x, y, or z direction.

As representative examples, the mode spectra for a three- ($N = 3$) and a seven- ($N = 7$) particle chain are shown in Fig. 2, with the x, z, and y modes arranged from left to right. Coupling between x and z modes can be clearly identified by multiple spectral lines having the same frequency following the method outlined in [21,22,28]. For example, in the seven-particle chain [Fig. 2(b)], at the resonant frequency of $x(6)$, $f \approx 16$ Hz, two light spectral lines corresponding to the $z(5)$ and $z(7)$ modes can be seen, implying that this mode is no longer a pure x mode, but rather a mode with mixed polarization, consisting of $x(6)$, $z(5)$, and $z(7)$ components. In other words, the $x(6)$ mode is coupled to both the $z(5)$ and $z(7)$ modes. Conversely, at the resonant frequencies of the $z(5)$ and $z(7)$ modes, $f \approx 20$ and 22 Hz respectively, two light spectral lines corresponding to the $x(6)$ mode can be found showing that the couplings

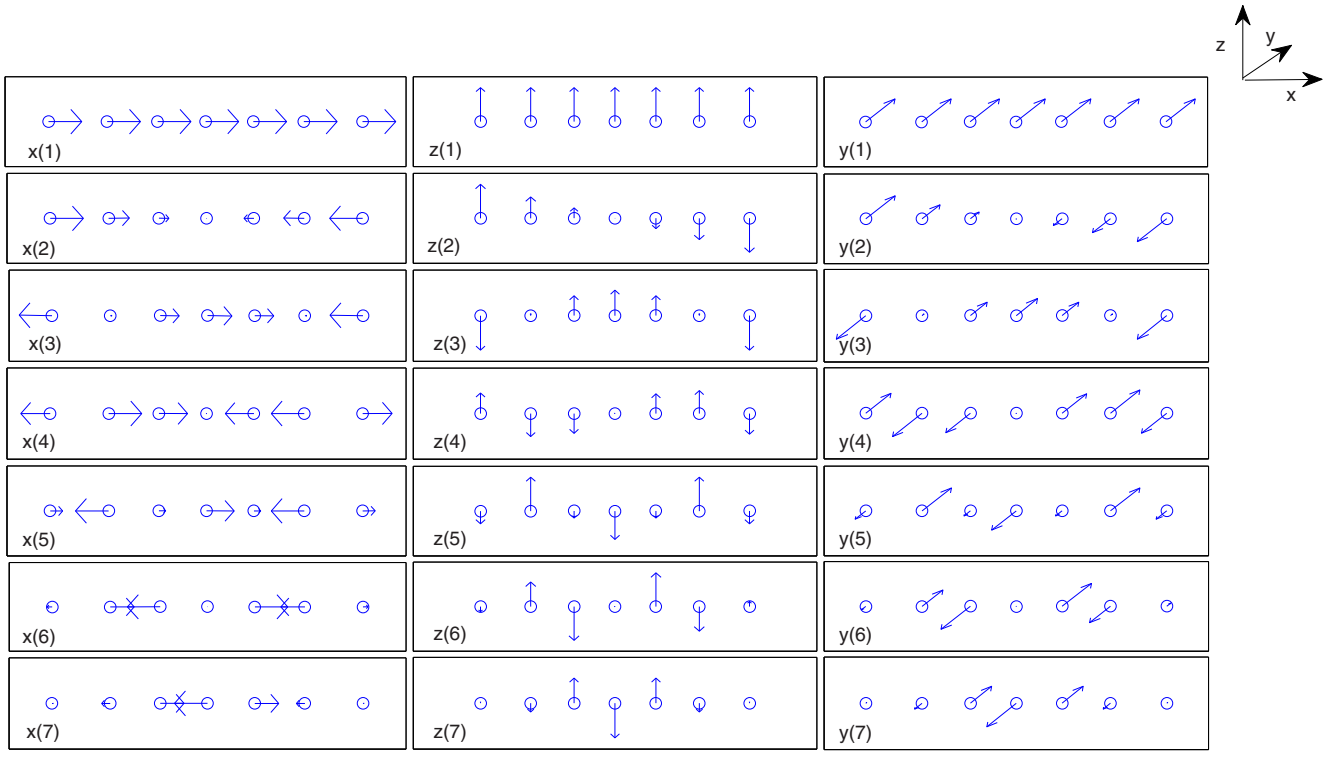

FIG. 1. (Color online) Eigenvectors for the x, z, and y modes for a seven-particle chain.

$x(6)z(5)$ and $x(6)z(7)$ are both mutual. The extra spectral lines resulting from these couplings form two additional branches in the mode spectrum and correspond to particle motion in the x and z directions, namely, the x_c and z_c branches.

By inspection of the mode spectra, coupling rules can be determined and shown to be different from those found for circular clusters [22,28]: (1) The y modes are not coupled with either x or z modes. This is in excellent agreement with the case for large 2D crystals, where the in-plane transverse DLW shows no coupling to other waves [9,23–25]. (2) Between x and z modes, coupling only occurs between modes having adjacent indices. That is, the mode x(i) [or z(i)] will only couple to $z(i \pm 1)$ [or $x(i \pm 1)$]. For $i = 0$ or N, coupling can only occur with a single mode since indices of -1 and $N+1$

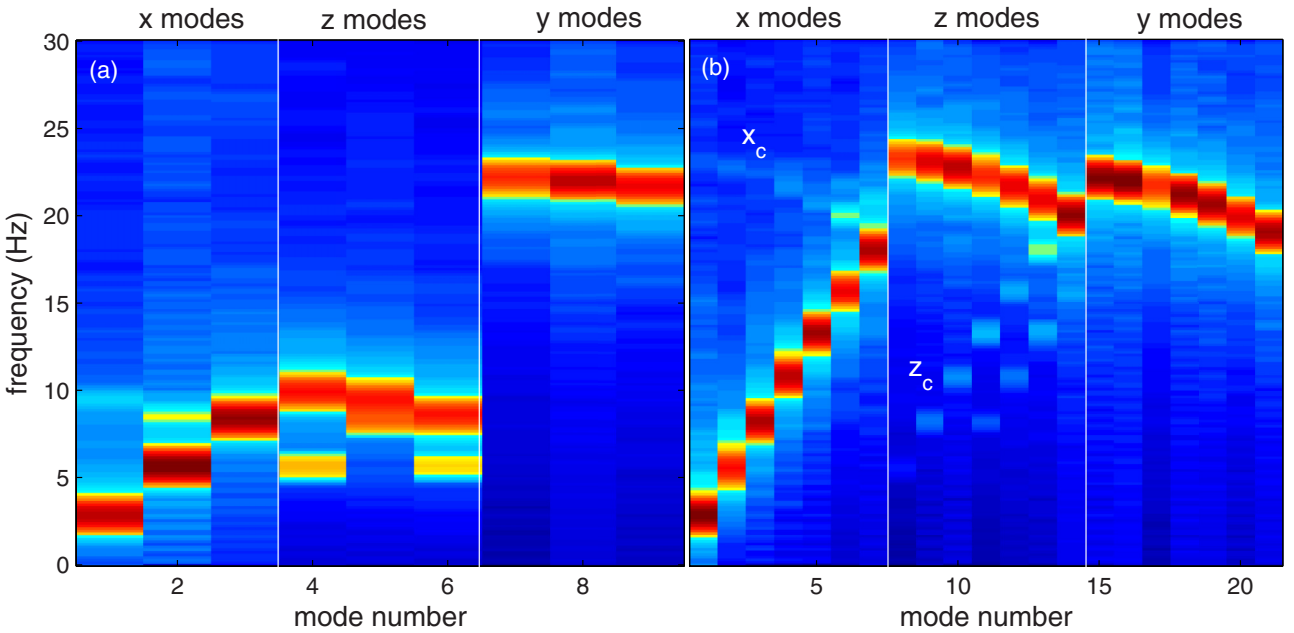

FIG. 2. (Color online) Normal mode spectra for a three-particle chain with (a) $E_z' = 6.0 \times 10^5$ V/m^{-2} and a seven-particle chain with (b) $E_z' = 3.3 \times 10^6$ V/m^{-2}.

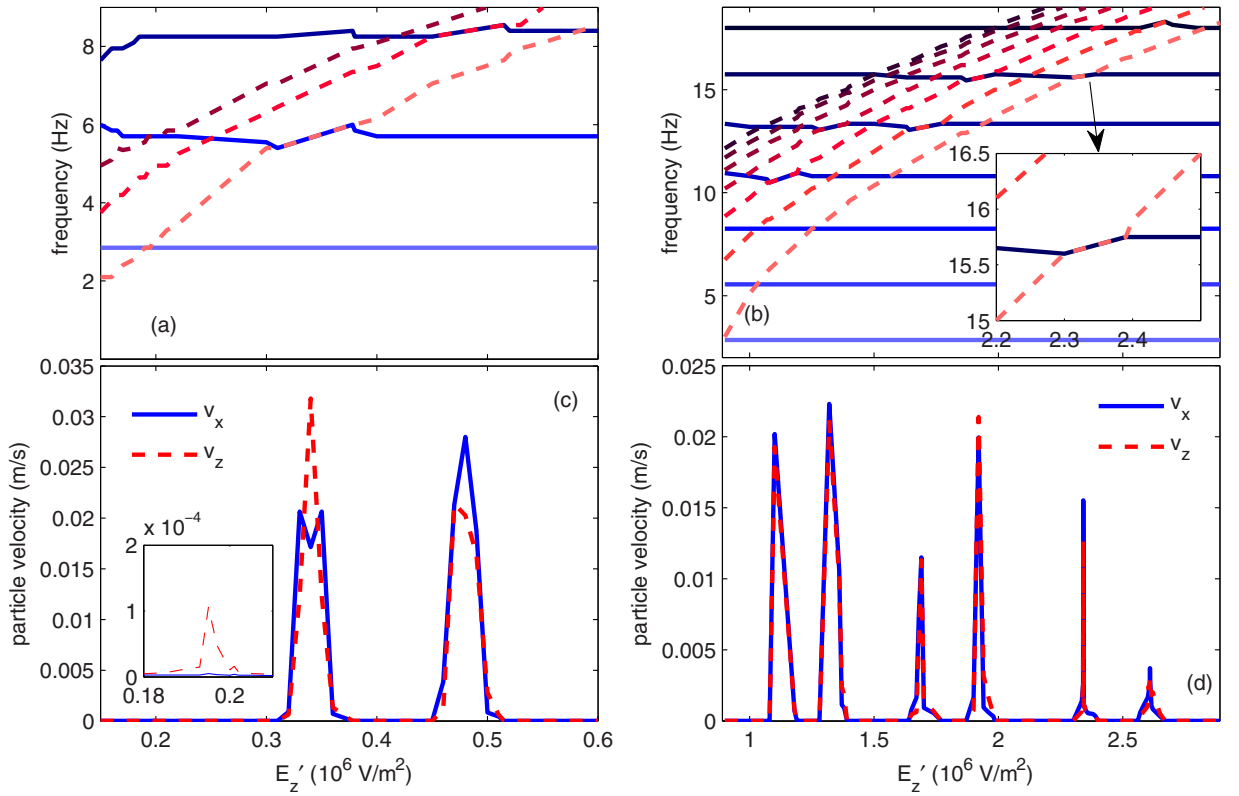

FIG. 3. (Color online) (a), (b) Normal mode frequencies and (c), (d) average particle velocities as functions of E_z' for a (a), (c) three- and (b), (d) seven-particle chain. In (a) and (b), x and z modes are represented by blue solid and red dashed lines, respectively. In (c) and (d), velocities in the x and z directions are represented by blue solid and red dashed lines, respectively.

are not allowed. (3) All couplings are mutual other than when a sloshing mode is involved. Whenever a sloshing mode couples to another mode, the sloshing mode remains pure while the mode being coupled to acquires a sloshing component. This unidirectional characteristic has also been observed for circular clusters [22].

B. Resonance instabilities and melting

To analyze the resonances between coupled modes having equal frequencies, simulations were conducted while varying E_z' and holding E_x' and E_y' constant. Using the three- and seven-particle chains as representative examples, the $E_z'-fr$ functions (frequency as a function of E_z') for the x and z modes are shown in Figs. 3(a) and 3(b). The x mode frequencies were found to remain constant while the z mode frequencies varied with E_z'. A lower limit for E_z' was established in order to maintain the 1D structure of the system; for E_z' values below this limit, the one-dimensional structure of the chain underwent the well-known zigzag transition [14].

For consistency with previous research, three types of resonances can be defined following the framework established in [22]. Type I is defined as resonances involving a sloshing mode. Due to its unidirectional characteristic as discussed above, this creates an instability for the sloshing mode only, namely a unidirectional instability. Type II resonances occur between two mutually coupled modes and their $E_z'-fr$ functions repel each other as they approach the intersection. This leads to a forbidden frequency gap but does not create instabilities. Type III resonances also occur between two mutually coupled modes but their $E_z'-fr$ functions are attractive and merge with one another as they approach the intersection, leading to instability for both modes, namely, a bidirectional instability.

In Figs. 3(c) and 3(d), the average particle velocities in the x and z directions are plotted as functions of E_z' with peaks exhibiting instabilities. Comparison of these results with Figs. 3(a) and 3(b) shows that each peak occurs at an

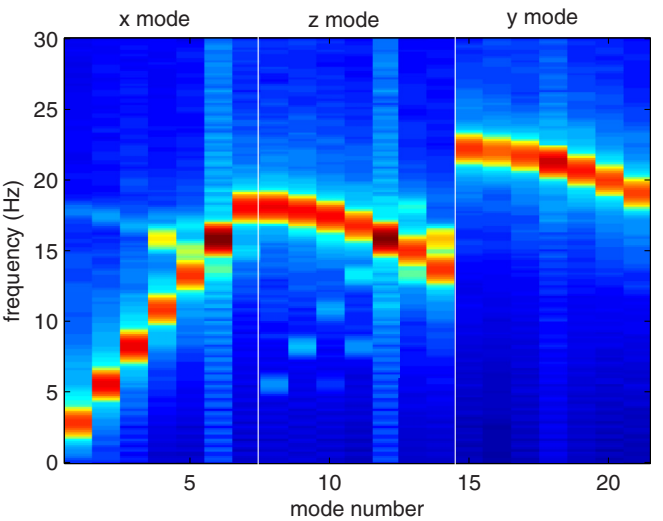

FIG. 4. (Color online) Normal mode spectra for a seven-particle chain with $E_z' = 1.985 \times 10^6$ V/m^{-2}.

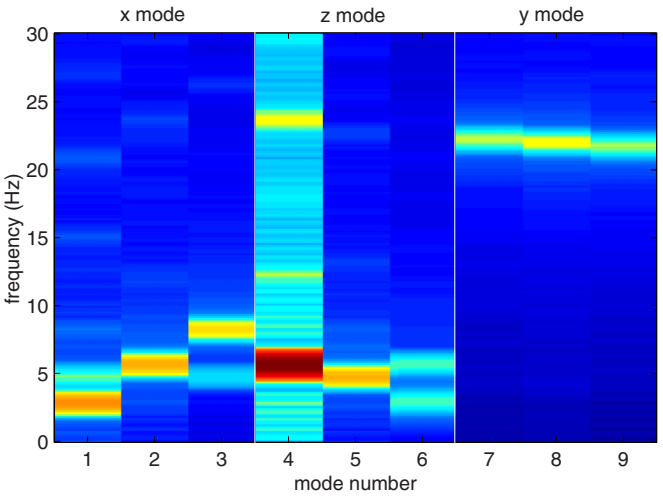

FIG. 5. (Color online) Normal mode spectra for a three-particle chain with $E_z' = 1.95 \times 10^5$ V/m^{-2}.

intersection between the $E_z' - fr$ functions for two coupled modes. A closer look shows that the $E_z' - fr$ functions are attractive and merge with each other as they approach the intersection [inset in Fig. 3(b)], with the width of the merged line equal to the width of the instability (the velocity peak) illustrating one characteristic of a Type III resonance. Furthermore, the bidirectional nature of the Type III resonance can be clearly seen in both particle velocity (Figs. 3(c) and 3(d) and spectral energy density (Fig. 4). The velocity increases in both the x and z directions, while the energy density increases for modes $x(6)$ and $z(5)$.

A Type I resonance occurs for a three-particle chain when the z sloshing mode and the $x(2)$ mode are equal in frequency as evidenced again by the increase in both spectral energy density (Fig. 5) and particle velocity [inset in Fig. 3(c)]. The unidirectional nature can be clearly seen in both with the energy density increasing only for the sloshing mode and the velocity increasing only in the z direction. As shown in Fig. 3(c), the velocity peak for a Type I resonance is two orders of magnitude lower than those for Type III, indicating that the coupling strength for Type I is much weaker than that for Type III, in agreement with the case for circular clusters [22]. Type II resonances have not been observed for one-dimensional chains.

As expected, nonequilibrium melting is observed induced by the resonance instabilities. Similar to the case of circular clusters [22], a Type I resonance is found to cause the system to vibrate as a whole without melting, while a Type III resonance will always cause melting provided the coupling strength is large enough. (This can be "tuned" numerically by varying the magnitude of the point charge q.) The melting "threshold" is identified by the transition from a state where all particles vibrate around their equilibrium positions to a state where particles are "hopping" between their equilibrium positions. This microscopic view has been employed in extensive research on finite system melting [30,34–37] and its agreement with the definition in terms of the (thermodynamic) phase space [34] can be seen in [30].

Following [22,43], the instantaneous relative interparticle distance fluctuation (IDF) $u_{\rm rel}$ was used to investigate the temporal evolution of the melting process. Due to the system's anisotropic characteristic, the instantaneous IDF in a specified direction is defined by

$$u_{{\rm rel}(\sigma)} = \frac{2}{N(N-1)} \sum_{1 \leqslant i \leqslant j}^{N} \frac{|\sigma_{ij} - \sigma_{ij0}|}{r_{ij0}}, \tag{3}$$

where σ can be x, y, or z; N is the particle number; $\sigma_{i,j}$ and $\sigma_{i,j0}$ are the instantaneous and equilibrium distances between particles i and j along the specified direction; and $r_{ij0} = \sqrt{x_{ij0}^2 + y_{ij0}^2 + z_{ij0}^2}$. As a representative example, Fig. 6 shows $u_{{\rm rel}(\sigma)}$ as a function of time for the melting of a seven-particle chain as induced by the $x(4)z(5)$ resonance instability. Similar to circular clusters, melting proceeds via a two-step process. (See the movie included in the Supplemental Material [44].)In the first step, particles exhibit growing oscillations with their velocity oriented along the direction of the eigenvectors of the excited modes. In the second step, starting at approximately 11 s, these vibrations become irregular with particles eventually exhibiting hopping between their equilibrium positions as indicated by a sudden increase in $u_{{\rm rel}(x)}$. (In this case, this occurs at approximately 12.2 s.) A similar two-step process has been reported for the melting of a 2D dust cluster triggered by the motion of a single particle hanging underneath the cluster [35].

It can be seen that $u_{{\rm rel}(x)}$ and $u_{{\rm rel}(z)}$ exhibit sudden increases at the same point in time, while the increase in $u_{i,{\rm rel}(y)}$ occurs at a later time. This agrees with the fact that the instability is induced by the x and z mode resonance. The growth rate of the regular oscillations occurring in the first stage of the process is usually different between the x and z motion, but the threshold of $u_{\rm rel}$, obtained by averaging the values of $u_{\rm rel}$ over the ten data frames collected immediately before particle hopping, is in the range of 0.1 ± 0.03 for both x and z motions (inset in Fig. 6). These values agree with those obtained for circular clusters [22] and are in excellent agreement with the Lindemann criterion for macroscopic Coulomb systems [43]. Therefore, the Lindemann criterion, which was originally used

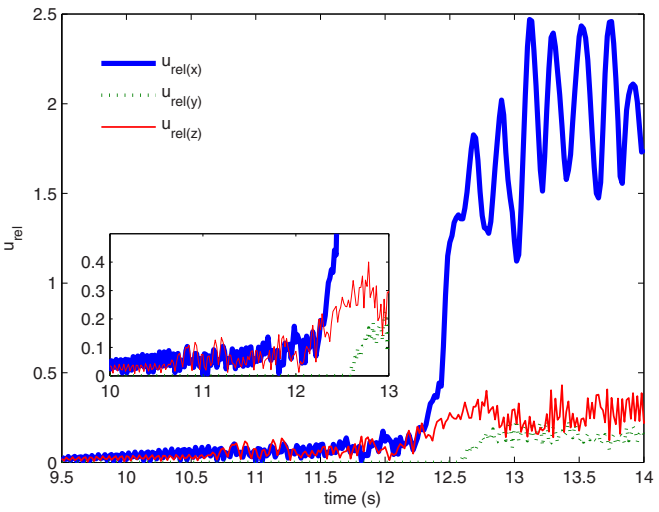

FIG. 6. (Color online) $u_{{\rm rel}(\sigma)}$ as a function of time for the melting of a seven-particle chain induced by the $x(4)z(5)$ resonance instability. $u_{{\rm rel}(\sigma)}$ in the x, z, and y directions is represented by blue thick lines, red thin lines, and green dotted lines, respectively.

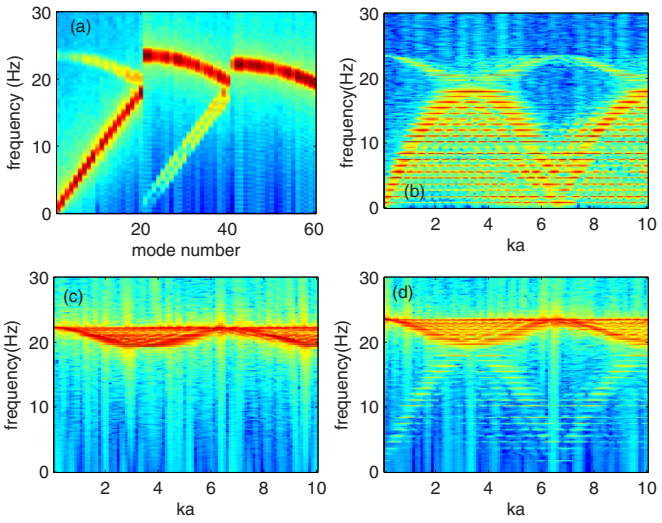

FIG. 7. (Color online) (a) Normal mode spectra for a 20-particle chain and the dispersion relations obtained from the spectra corresponding to the (b) x, (c) y, and (c) z modes.

for equilibrium melting driven by temperature increase, is also suitable for nonequilibrium melting driven by resonance instabilities, even for extremely anisotropic systems such as dust chains within a complex plasma.

C. Relationship between normal modes and dispersion relations

As mentioned above, a horizontal dust chain exhibits mode eigenvectors resembling a series of nonuniform standing waves with differing numbers of unequal wavelengths; therefore, it can be employed as a model for examination of the relationship between the normal modes arising within finite systems and the dispersion properties of larger systems. For this purpose, we conducted a simulation of horizontal chains comprised of 20 particles. As can be seen in the normal mode spectrum [Fig. 7(a)], the x, y, z and x_c, z_c branches are similar to the case found for chains having fewer particles (Fig. 2). The dispersion relations for DLWs [Figs. 7(b)–7(d)] can be obtained by multiplying the mode spectra matrix by the transition matrix defined by

$$U_{n,k(\sigma)} = \sum_{i=1}^{N} e_{i,n(\sigma)} e^{-ikx_i}, \tag{4}$$

where $e_{i,n(\sigma)}$ is the eigenvector for the nth σ mode at particle position i (where σ can be x, y, or z), and k is a specified wave number. Figures 7(b)–7(d) show the dispersion relations obtained from the x, y, and z modes and correspond to the longitudinal, in-plane, and out-of-plane transverse DLWs, respectively. As shown, the in-plane transverse DLW exhibits optical wave characteristics and shows no coupling to other waves, in agreement with previous research [9,23–25,45]. The longitudinal and out-of-plane transverse waves exhibit curved dispersion relations with rising and falling branches, similar to those observed experimentally and numerically for 2D [10–14,18,23–25] and 1D [12,45] structures. In particular, the additional dispersion branches induced by coupling as

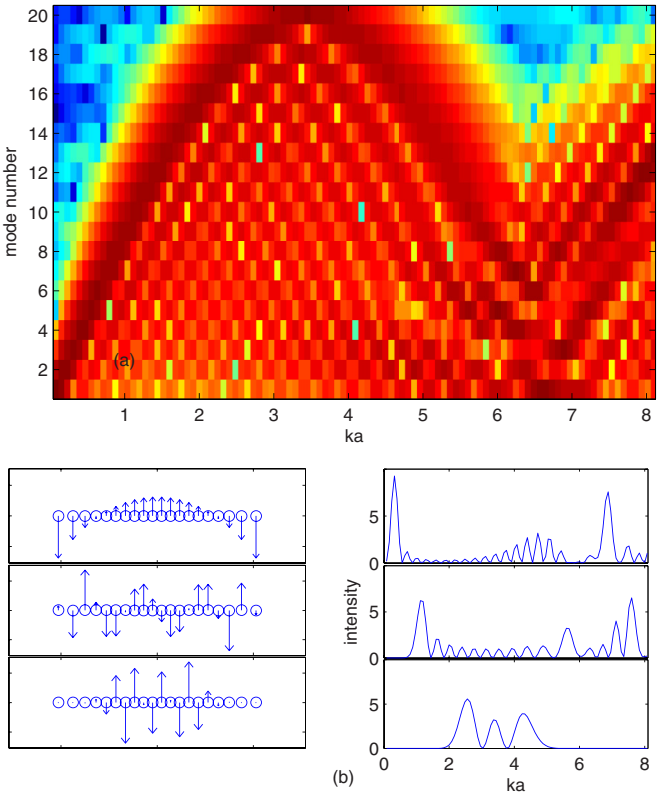

FIG. 8. (Color online) (a) The transition matrix for a 20-particle horizontal chain as defined by Eq. (4) in the text. (b) The eigenvectors for the third, tenth, and 18th normal modes (left panel) and corresponding intensity over k in the transition matrix (right panel).

observed in previous experiments [18,23–25] can be clearly seen.

On the other hand, the dispersion relations also exhibit characteristics that are different from those observed in large crystals. The first of these is that the curves appear to be formed in discrete stripes within the frequency regime. This is obviously caused by the finite nature of the system; there are exactly 20 stripes having frequencies equal to the 20 normal modes. Secondly, the energy densities between the rising and falling branches show a much stronger fluctuation than those observed in larger systems.

Both the similarities and differences discussed above can be explained by plotting the transition matrix directly (Fig. 8). The transition matrix $U_{n,k}$ represents the transformation between the two bases, the normal mode eigenvectors, and the Fourier series in k space. Thus, the intensity in any given row is obtained by Fourier transformation [Eq. (4)] of each mode's eigenvectors over x. The transition from an almost linear structure of mode spectra [as seen in Fig. 7(a)] to a curved structure of dispersion relations [Figs. 7(b)–7(d)] can be easily understood by noting the curved (nonlinear) relationship between the mode number n and wave number k shown in Fig. 8(a). The matrix also exhibits strong intensity fluctuations over k for each normal mode. This can be seen more clearly by plotting the intensity over k for specified modes. Figure 8(b) shows this intensity for the third, tenth, and 18th normal modes alongside their eigenvectors. Since a mode with an

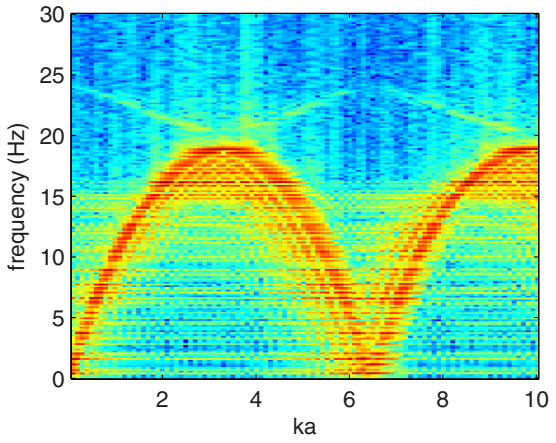

FIG. 9. (Color online) The longitudinal dispersion relation obtained by inspection of the middle 20 particles within a 50-particle chain.

ideal sinusoidal wave structure would result in a single sharp peak in its intensity over k, the series of peaks seen in Fig. 8(b) are caused by the nonuniform wave structure of the normal modes, which are in turn induced by the finite nature of the system. This conclusion is supported by comparison with the dispersion relations obtained from the central section of a simulated larger chain. Figure 9 shows the longitudinal dispersion relation obtained by inspection of the middle 20 particles in a 50-particle chain. A sharper, more continuous dispersion curve and reduced energy-density fluctuation can be seen, thus verifying the observed discontinuity and fluctuation to be directly related to the finite nature of the system.

Finally, the normal mode spectra for a 20-particle chain were examined upon the crossing of the x and z mode branches [Fig. 10(a)]. The dispersion relations for the longitudinal [Fig. 10(b)] and out-of-plane transverse DLWs [Fig. 10(c)] were obtained employing the transition matrix. They clearly resemble those observed previously in large crystals [18,23–25], with the hybrid mode indicated by the high-energy-density region at the intersection between the DLWs. It is important to note that there is a difference between the mode resonance for the 20-particle chain and chains having fewer particles (Figs. 4 and 5). Since the frequency difference between adjacent modes in a 20-particle chain is much smaller, overlap between adjacent instabilities occurs at the resonance point. For example, the high-energy-density region in Fig. 10 spans the $x(16)z(17)$ and $x(17)z(16)$ resonances. (The enhanced energy density at other mode numbers may be due to additional overlapping resonances or nonlinear effects.) Further increase in particle numbers above 20 results in much more prominent overlap between individual instabilities. Therefore, in large crystals, the k range where the hybrid mode emerges upon mode coupling usually spans more than several resonances and is roughly determined by the coupling strength, or the effective dipole moment of the wake [25]. This resonance overlap leads to the conclusion that only one unstable region should be observed for larger plasma crystals, rather than the discrete instabilities observed in finite systems [21,22,28].

IV. CONCLUSIONS

In summary, the normal modes for a finite, 1D horizontal dust chain in complex plasma were investigated employing a numerical simulation. Simulations were conducted for chains comprised of three to 20 dust particles, taking into account ion flow within the sheath using the point charge model. Mode couplings were identified in the mode spectra with coupling rules determined to be (1) Y modes are not coupled with either the x or z modes, (2) between x and z modes, coupling occurs only between modes having adjacent indices, and (3) couplings are mutual except for cases where a sloshing mode is involved.

Whenever two coupled modes have equal frequencies, resonance instabilities occur. Two types of resonance instabilities were found for a 1D chain structure—a bidirectional instability induced by resonance between two mutually coupled modes and a unidirectional instability induced by resonance involving a sloshing mode. Similar to the case for circular clusters, a bidirectional instability can cause melting of the structure provided the coupling is strong enough. For this case, melting

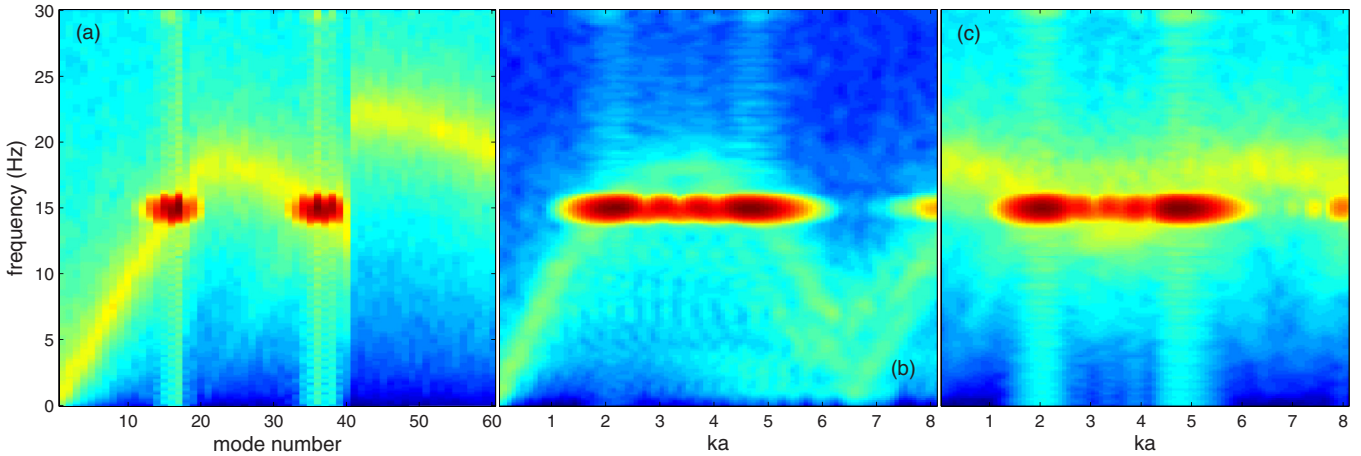

FIG. 10. (Color online) (a) Normal mode spectra for a 20-particle chain and the dispersion relations obtained from the spectra corresponding to the (b) x and (c) z modes upon the crossing of the x and z mode branches.

proceeds via a two-step process and obeys the Lindemann criterion.

Additionally, the relationship between the normal modes and the wave dispersion relations was studied. The dispersion relation was obtained through multiplication of the mode spectra matrix by a transition matrix. The resulting dispersion relations were not only found to resemble those observed in large crystals, they also were shown to exhibit characteristics unique to finite systems, such as the discontinuity in frequency and a strong energy-density fluctuation. The hybrid mode upon the crossing of the x and z mode branches was also found to resemble results for large crystals and the wave number range it spans can be explained by overlapping between resonances.

Finally, it is worth noting that these predictions should be relatively easy to examine experimentally, considering that typical experimental values were chosen for the particle charge, mass, screening length, and confinement [28]. If true, complex plasma dust chains may well prove an excellent analog for the experimental examination on macroscopic time and length scales of mode coupling in other chainlike microscopic complex systems such as polyatomic molecules and proteins. This research is underway and will be reported in an upcoming publication.

[1] T. Uzer, Phys. Rep. **199**, 73 (1991).
[2] B. C. Dian, A. Longarte, and T. S. Zwier, Science **296**, 2369 (2002).
[3] N. Bozinovic, Y. Yue, Y. Ren, M. Tur, P. Kristensen, H. Huang, A. E.Willner, and S. Ramachandran, Science **340**, 1545 (2013).
[4] J. Resovsky and M. Ritzwoller, Geophys. Res. Lett. **22**, 2301 (1995).
[5] I. U Uzun-Kaymak, P. N. Guzdar, S. Choi, M. R. Clary, R. F. Ellis, A. B. Hassam, and C. Teodorescu, Europhys. Lett. **85**, 15001 (2009).
[6] J. Ford and Gary H. Lunaford, Phys. Rev. A **1**, 59 (1970).
[7] L. E. Reichl, *A Modern Course in Statistical Physics*, 3rd ed. (Wiley, Weinheim, 2009).
[8] A. V. Ivlev and G. Morfill, Phys. Rev. E **63**, 016409 (2000).
[9] S. K. Zhdanov, A. V. Ivlev and G. E. Morfill, Phys. Plasmas **16**, 083706 (2009).
[10] A. Homann, A. Melzer, S. Peters, R. Madani, and A. Piel, Phys. Lett. A **242**, 173 (1998).
[11] S. Nunomura, J. Goree, S. Hu, X. Wang, A. Bhattacharjee, and K. Avinash, Phys. Rev. Lett. **89**, 035001 (2002).
[12] S. V. Vladimirov, Phys. A **315**, 222 (2002).
[13] K. Qiao and T. W. Hyde, Phys. Rev. E **68**, 046403 (2003).
[14] K. Qiao and T. W. Hyde, Phys. Rev. E **71**, 026406 (2005).
[15] S. V. Vladimirov and M. Nambu, Phys. Rev. E **52**, R2172 (1995).
[16] F. Melandsø and J. Goree, Phys. Rev. E **52**, 5312 (1995).
[17] G. A. Hebner and M. E. Riley, Phys. Rev. E **68**, 046401 (2003).
[18] B. Liu, J. Goree, and Y. Feng, Phys. Rev. Lett. **105**, 085004 (2010).
[19] V. A. Schweigert, I. V. Schweigert, A. Melzer, A. Homann, and A. Piel, Phys. Rev. E **54**, 4155 (1996).
[20] V. V. Yaroshenko, S. V. Vladimirov, and G. E. Morfill, New J. Phys. **8**, 201 (2006).
[21] K. Qiao, J. Kong, Z. Zhang, L. S. Matthews, and T. W. Hyde, IEEE Trans. Plasma Sci. **41**, 745 (2013).
[22] K. Qiao, J. Kong, E. V. Oeveren, L. S. Matthews, and T. W. Hyde, Phys. Rev. E **88**, 043103 (2013).
[23] L. Couëdel, V. Nosenko, A. V. Ivlev, S. K. Zhdanov, H. M. Thomas, and G. E. Morfill, Phys. Rev. Lett. **104**, 195001 (2010).
[24] L. Couëdel, S. K. Zhdanov, A. V. Ivlev, V. Nosenko, H. M. Thomas, and G. E. Morfill, Phys. Plasmas **18**, 083707 (2011).
[25] A. V. Ivlev, V. Nosenko, and T. B. Röcker, Contrib. Plasma Phys. **55**, 35 (2015).
[26] A. V. Ivlev, U. Konopka, G. Morfill, and G. Joyce, Phys. Rev. E **68**, 026405 (2003).
[27] R. Kompaneets, S. V. Vladimirov, A. V. Ivlev, V. Tsytovich, and G. Morfill, Phys. Plasmas **13**, 072104 (2006).
[28] K. Qiao, J. Kong, J. Carmona-Reyes, L. S. Matthews, and T. W. Hyde, Phys. Rev. E **90**, 033109 (2014).
[29] J. P. Schiffer, Phys. Rev. Lett. **88**, 205003 (2002).
[30] J. Boning, A. Filinov, P. Ludwig, H. Baumgartner, M. Bonitz, and Y. E. Lozovik, Phys. Rev. Lett. **100**, 113401 (2008).
[31] A. V. Filinov, M. Bonitz, and Y. E. Lozovik, Phys. Rev. Lett. **86**, 3851 (2001).
[32] D. J. Wineland, J. C. Bergquist, W. M. Itano, J. J. Bollinger, and C. H. Manney, Phys. Rev. Lett. **59**, 2935 (1987).
[33] D. D. Frantz, J. Chem. Phys. **115**, 6136 (2001).
[34] A. Proykova and R. S. Berry, J. Phys. B **39**, R167 (2006).
[35] Yuriy Ivanov and Andre Melzer, Phys. Plasmas **12**, 072110 (2005).
[36] A. Melzer, A. Schella, J. Schablinski, D. Block, and A. Piel, Phys. Rev. Lett. **108**, 225001 (2012).
[37] A Melzer, A. Schella, J. Schablinski, D. Block, and A. Piel, Phys. Rev. E **87**, 033107 (2013).
[38] B. Liu, K. Avinash, and J. Goree, Phys. Rev. E **69**, 036410 (2004).
[39] E. B. Tomme, B. M. Annaratone, and J. E. Allen, Plasma Sources Sci. Technol. **9**, 87 (2000).
[40] D. Richardson, Mon. Not. R. Astron. Soc. **269**, 493 (1994).
[41] L. S. Matthews, K. Qiao, and T. W. Hyde, Adv. Space Res. **38**, 2564 (2006).
[42] A. Melzer, Phys. Rev. E **67**, 016411 (2003).
[43] R. D. Etters and J. Kaelberer, Phys. Rev. A **11**, 1068 (1975).
[44] See Supplemental Material at http://link.aps.org/supplemental/10.1103/PhysRevE.91.053101 for melting of a seven-particle chain induced by the $x(4)z(5)$ resonance.
[45] B. Liu, K. Avinash, and J. Goree, Phys. Lett. **91**, 255003 (2003).